Pharmacokinetic modelling to estimate intracellular favipiravir ribofuranosyl-5′-triphosphate exposure to support posology for SARS-CoV-2

Henry Pertinez[1,2], Rajith KR Rajoli[1,2], Saye H Khoo[1,2], Andrew Owen[1,2].

[1]Department of Pharmacology and Therapeutics, Materials Innovation Factory, University of Liverpool, Liverpool, L7 3NY, UK
[2]Centre of Excellence in Long acting Therapeutics (CELT), University of Liverpool, Liverpool, L69 3BX, UK

Author for correspondence:
Professor Andrew Owen
Department of Pharmacology and Therapeutics
Materials Innovation Factory
University of Liverpool
51 Oxford Street,
Liverpool L7 3NY
United Kingdom
Email - aowen@liverpool.ac.uk
Phone - +44 (0)151 795 7129
Key words: COVID-19, SARS-CoV-2, Coronavirus, Pharmacokinetics, intracellular, active metabolite

Conflicts of interest statement
AO is a Director of Tandem Nano Ltd and co-inventor of patents relating to drug delivery. AO has received research funding from ViiV, Merck, Janssen and consultancy from Gilead, ViiV and Merck not related to the current paper. No other conflicts are declared by the authors.

Funding
The authors received no funding for the current work. AO acknowledges research funding from EPSRC (EP/R024804/1; EP/S012265/1), NIH (R01AI134091; R24AI118397), European Commission (761104) and Unitaid (project LONGEVITY).

Abstract

Background: The role of favipiravir as a treatment for COVID-19 is unclear, with discrepant activity against SARS-CoV-2 *in vitro*, concerns about teratogenicity and pill burden, and an unknown optimal dose. In Vero-E6 cells, high concentrations are needed to inhibit SARS-CoV-2 replication. The purpose of this analysis was to use available data to simulate intracellular pharmacokinetics of favipiravir ribofuranosyl-5□-triphosphate (FAVI-RTP) to better understand the putative applicability as a COVID-19 intervention.

Methods: Previously published *in vitro* data for the intracellular production and elimination of FAVI-RTP in MDCK cells incubated with parent favipiravir was fitted with a mathematical model to describe the time course of intracellular FAVI-RTP concentrations as a function of incubation concentration of parent favipiravir. Parameter estimates from this model fitting were then combined with a previously published population PK model for the plasma exposure of parent favipiravir in Chinese patients with severe influenza (the modelled free plasma concentration of favipiravir substituting for *in vitro* incubation concentration) to predict the human intracellular FAVI-RTP pharmacokinetics.

Results: *In vitro* FAVI-RTP data was adequately described as a function of *in vitro* incubation media concentrations of parent favipiravir with an empirical model, noting that the model simplifies and consolidates various processes and is used under various assumptions and within certain limits. Parameter estimates from the fittings to *in vitro* data predict a flatter dynamic range of peak to trough for intracellular FAVI-RTP when driven by a predicted free plasma concentration profile.

Conclusion: This modelling approach has several important limitations that are discussed in the main text of the manuscript. However, the simulations indicate that despite rapid clearance of the parent drug from plasma, sufficient intracellular FAVI-RTP may be maintained across the dosing interval because of its long intracellular half-life. Population average intracellular FAVI-RTP concentrations are estimated to maintain the Km for the SARS-CoV-2 polymerase for 3 days following 800 mg BID dosing and 9 days following 1200 mg BID dosing after a 1600 mg BID loading dose on day 1. Further evaluation of favipiravir as part of antiviral combinations for SARS-CoV-2 is warranted.

Introduction

The urgent global public health threat posed by COVID-19 has led the global scientific community to rigorously explore opportunities for repurposing existing medicines based upon either demonstration of auspicious antiviral activity against SARS-CoV-2, or a plausible mechanistic basis for anti-inflammatory / immunomodulatory activity. If sufficiently potent antiviral agents can be identified, there is potentially significant opportunity for deployment either as prophylaxis or in early infection to prevent development of severe disease. The role of antivirals in later stages of COVID-19 is less clear but cannot be rigorously assessed until sufficiently potent antiviral drug combinations become available. Several groups have highlighted the importance of considering the fundamental principles of clinical pharmacology when selecting candidates for investigation as antiviral agents [1-3], including a nuanced understanding of the principles of plasma protein binding [4]. For most successful antiviral drugs developed to date, a key principle is that plasma drug concentrations be maintained above *in vitro*-defined target concentrations (EC_{90} or protein binding adjusted EC_{90} where available) for the duration of the dosing interval. However, where the drug target resides intracellularly, and generation of an intracellular active metabolite is a prerequisite to unmask the pharmacophore, a more thorough understanding of the intracellular pharmacokinetics is required to rationalise doses required to maintain antiviral activity. For example, nucleoside-based drugs or prodrugs require intracellular phosphorylation by a cascade of host proteins, to generate tri-phosphorylated metabolites that exert the activity on the viral polymerase [5, 6]. Indeed, antiviral nucleoside analogues for HIV (e.g. tenofovir alafenamide), HCV (sofosbuvir) and several of the repurposing opportunities for SARS-CoV-2 (e.g. remdesivir) have active triphosphate metabolites with intracellular half-lives much longer than the parent drug in plasma [7-9]. Therefore, for many nucleosides being explored for SARS-CoV-2 (including favipiravir, molnupiravir), the activity may be maintained across the dosing interval despite plasma concentrations of the parent dropping below the EC_{90} at trough concentration (C_{trough}).

Favipiravir is approved for influenza in Japan but not elsewhere and has been intensively studied as a potential antiviral intervention for several other RNA viruses; most recently SARS-CoV-2. For several reasons, considerable uncertainty exists about the suitability of favipiravir as a COVID-19 intervention. Concerns about teratogenicity and high pill burden may limit widespread uptake of the drug during early infection, particularly in the absence of concomitant contraceptive use in women of child-bearing age [10]. Furthermore, *in vitro* studies of favipiravir in Vero-E6 cell infected with SARS-CoV-2 have yielded inconsistent findings[11-14], and low potency (EC_{90} = 159 µM; 24.9 µg/mL) has been described in those studies that have shown activity [14]. Favipiravir plasma concentrations

also appear to diminish, the longer that patients receive the medicine [10], and studies in severe COVID-19 disease have shown that plasma exposures are almost entirely abolished [15]. Despite the uncertainty and potential limitations, favipiravir has been demonstrated to exert antiviral activity against SARS-CoV-2 in the Syrian Golden Hamster model [16], and despite extremely high doses (1000 mg/kg intraperitoneally), C_{trough} values in this model were similar to those achieved in human studies of influenza (4.4 µg/ml in hamster versus 3.8 µg/ml day 10 trough in human; [16, 17]). Cell-free models have also demonstrated the ability of the intracellular ribofuranosyl-5′-triphosphate metabolite (FAVI-RTP) to directly inhibit the SARS-CoV-2 polymerase [18].

The purpose of this work was to model from published plasma pharmacokinetic profiles, the likely concentrations of the intracellular active moiety (FAVI-RTP) and evaluate whether putative target concentrations necessary to inhibit SARS-CoV-2 can be pharmacologically attained in humans.

Methods

Prior In-Vitro Data

Data for the intracellular formation and catabolism of intracellular favipiravir-RTP (FAVI-RTP) in MDCK cells following incubation with parent favipiravir were digitised from previously published work [19]. Briefly, the *in vitro* experiments carried out by Smee et al. involved incubation of confluent layers of MDCK cells in T-25 flasks with media containing favipiravir at 32, 100, 320 or 1000 μM for varying durations. Smee et al. included 10% foetal bovine serum in media and plasma protein binding of favipiravir is relatively low in humans (54%; [10]). Therefore, given that the protein concentration in the media was low in these incubations, it was assumed that the nominal *in vitro* media concentrations of favipiravir for the incubations equated to the free drug concentrations.

At given timepoints, medium was removed, and cells were washed, lysed and FAVI-RTP was quantified in the lysate using HPLC with UV detection. For catabolism/elimination experiments MDCK cells were incubated with favipiravir containing media at the specified concentrations for 24h to allow production and accumulation of FAVI-RTP, before the media was removed and replaced with favipiravir-free media. Incubation then continued for a series of timepoints at which media was removed, and cell lysate was assayed for FAVI-RTP. Smee et al. present their FAVI-RTP quantification in normalised units of pmol/10^6 cells according to the cell counts of the incubations, which was taken to represent the normalised intracellular *amount* of FAVI-RTP. In this work a value provided by Bitterman et al. [20] for the volume of an MDCK cell as 2.08 pL was then used to convert the FAVI-RTP quantification of Smee et al. to units of pmol/(10^6 pL) = pmol/μL = μM.

Modelling of In-Vitro Data

The data for intracellular production and elimination of FAVI-RTP were fitted with a mathematical model in the R programming environment (v 4.0.3) [21] to describe and parameterise the observed data as a function of the incubation media concentrations and time. This fitting made use of the Pracma library [22] and lsqnonlin function for nonlinear regression.

Data for intracellular production (in presence of favipiravir containing media) and elimination of FAVI-RTP elimination (on removal of favipiravir containing media after a 24h incubation and replacement with blank media) were combined into single time courses for each medium concentration, to then be described with the following ordinary differential (rate) equation mathematical model:

144 Equation 1: $d[\text{FAVI-RTP}]_{cell}/dt = k_{in} * [\text{FAVI}]_{media} - k_{out} * [\text{FAVI-RTP}]_{cell}$

145

146 Where [ ] denotes concentration. The initial condition for $[\text{FAVI-RTP}]_{cell}$ is set to zero at time zero
147 and $[\text{FAVI}]_{media}$ switched to equal zero at the 24h timepoint to end the production rate of FAVI-RTP
148 and allow only the elimination rate to describe observed, declining concentrations from that time
149 forward. The parameter k_{in} has units of $time^{-1}$ and simultaneously describes net influx/diffusion of
150 parent favipiravir from media into the cell and its (net) subsequent conversion to FAVI-RTP. The use
151 of k_{in} therefore simplifies a more detailed description of favipiravir net influx into cells and
152 conversion into FAVI-RTP into an empirical 1^{st} order process dependent on media concentration of
153 favipiravir, to enable use of the information in the available data, where parent favipiravir itself is
154 not quantified.

155

156 Smee et al. do not explicitly quote the volume of media used in their incubations, but given the T-25
157 flasks used, a media volume of 5-10 ml could be expected. Across the lowest to highest favipiravir
158 media concentrations in the data (32 and 1000 µM), this therefore translates to a range of 0.16 to 10
159 µmol favipiravir present in the incubations at time = 0. The maximum amount of intracellular FAVI-
160 RTP produced after 24h in the 1000 µM incubation was 332 pmol / 10^6 cells ; with incubations
161 declared to contain approximately 7 x 10^6 cells on average, this gives a maximum total amount of
162 2,324 pmol = 2.3 nmol FAVI-RTP converted from favipiravir in 1:1 stoichiometry, which is << 1 %
163 conversion of the total amount of favipiravir available in the 1000 µM incubation at the start (with
164 similar calculations demonstrable at the other media concentrations). Therefore the $[\text{FAVI}]_{media}$
165 term in Equation 1 can be considered approximately constant for a given time course dataset of
166 incubations at a specified favipiravir concentration. In turn, this renders Equation 1 equivalent to a
167 zero order constant input model with first order elimination and with the zero order input being
168 switched off at 24h when media containing favipiravir was replaced with blank media.

169

170 ***In-vivo Intracellular Simulations***

171 The model and parameter estimates from the fitting to *in vitro* intracellular data, describing
172 intracellular FAVI-RTP concentrations as a function of the media incubation concentrations were
173 then taken forward and combined with a population PK model for plasma exposure for favipiravir
174 described by Wang et al. in a Chinese population receiving the drug for influenza [17], substituting
175 the media incubation concentration driving the intracellular FAVI-RTP production rate with the free
176 plasma concentration predicted by the population PK model. This provided a prospective simulation

177 of *in vivo* intracellular concentrations of FAVI-RTP (assuming cells of similar disposition to MDCK
178 cells) as a function of *in vivo* plasma exposure.
179
180 The population PK model of Wang et. al is a 1-compartment PK disposition model with 1st order
181 absorption. Therefore, the equations for the model for *in vivo* intracellular simulations were as
182 follows:
183
184 Equation 2: $d A_{Favi\_depot} / dt = -k_a * A_{Favi\_depot}$
185 Equation 3: $d [FAVI]_{plasma} / dt = (k_a * A_{Favi\_depot} - CL * [FAVI]_{plasma})/V$
186 Equation 4: $d [FAVI\text{-}RTP]_{cell} / dt = (k_{in} * [FAVI]_{plasma} * Fu_{plasma}) - k_{out} * [FAVI\text{-}RTP]_{cell}$
187
188 Where [ ] denotes concentration, CL and V are apparent values CL/F and V/F, and k_{in} and k_{out} used
189 values derived from the *in vitro* model fitting. The Wang et al. model also incorporated a time
190 dependent effect on CL, representative of favipiravir autoinduction of its own elimination, where:
191
192 Equation 5: $CL = CL_{day\_0} * (1+ 0.0614 * \text{days of dosing})$
193
194 The model assumes a minimal proportion of the total mass balance of favipiravir transfers in from
195 the plasma before conversion into the intracellular FAVI-RTP (similar to how the *in vitro* model
196 assumes a constant $[FAVI]_{media}$) and was therefore similar in some respects to a PKPD effect
197 compartment model.
198
199 PK parameter population interindividual variabilities estimated by Wang et al. were used to simulate
200 a population of 1000 sets of PK parameters and their resultant predicted $[FAVI]_{plasma}$ and $[FAVI\text{-}$
201 $RTP]_{cell}$ profiles, from which 90% prediction interval profile envelopes were calculated. No population
202 distribution of body weight was incorporated into this simulation which is equivalent therefore to
203 assuming each simulated subject had a body weight of 70kg according to the Wang et al. population
204 PK model. No interindividual variability in the k_{in} or k_{out} parameters was available or assumed.
205 Parameter values used, and their inter-individual variabilities, quoted from the population PK model
206 of Wang et al. are provided in Table 2, with Fu_{plasma} set at 0.46 [10].
207

Results

Modelling of In-Vitro Data

Data from the observed $[FAVI\text{-}RTP]_{cell}$ from Smee et al. at the four media concentrations investigated, overlaid with the model fittings are given in Figure 1, with parameter estimates and associated % relative standard errors in Table 1. The model was deemed to provide a satisfactory description of the observed data with acceptable precision of parameter estimates. However, it should be noted that k_{in} were not observed to be constant across the media incubation concentrations. A plot of k_{in} vs. $[FAVI]_{media}$ (the latter on a log-scale) is provided in Figure 2, indicating that some form of saturable relationship is most likely present, which may require an E_{max} type model to be accurately described over the full range of media concentrations. However, with data available at only four media concentrations there was insufficient information to adequately fit such a saturable model. A log-linear model has therefore been fitted instead to the log-linear portion of the k_{in} vs. $[FAVI]_{media}$ curve (the $[FAVI]_{media}$ range from 32 to 320 µM, which also encompasses a typical range of *in vivo* plasma concentrations under standard human dosing regimens) and is overlaid in Figure 2, where:

Equation 6: $$k_{in} = \ln([FAVI]_{media}) * k_{in\_slope} + k_{in\_intercept}$$

The values of k_{in_slope} and $k_{in\_intercept}$ were then taken forward to the *in vivo* simulations instead of a mean value of k_{in}, or the value from one $[FAVI]_{media}$ fitting alone, and were used via Equation 6 during simulations to calculate the value of k_{in} required for any free plasma concentration at any given time as an input parameter value for Equation 4. k_{out} estimates from fittings were consistent at the 4 i*n vitro* $[FAVI]_{media}$ concentrations. Therefore, the mean of the 4 estimates (0.108 h^{-1}) was taken as the input value for simulations using Equation 4.

In-vivo Intracellular Simulations

Simulations of predicted *in vivo* plasma and intracellular exposures for favipiravir and FAVI-RTP are shown in Figure 3A for a dosing regimen of 1600 mg BID loading dose for day 1, followed by 800 mg BID maintenance dosing for 9 further days. Simulations of predicted *in vivo* plasma and intracellular exposures for favipiravir and FAVI-RTP are shown in Figure 3B for a dosing regimen of 1600 mg BID loading dose for day 1, followed by 1200 mg BID maintenance dosing for 9 further days. In both cases, reference to the Km (Michaelis–Menten constant) for FAVI-RTP against the SARS-CoV-2 RNA-dependent RNA polymerase (RdRp) enzyme [18] is overlaid. The plasma target exposure based on *in vitro* EC_{90} for favipiravir of 159 µM against SARS-CoV-2 [14] is also shown but should be interpreted

242 with caution owing to the lack of clarity in *in vitro* free drug concentrations and whether human
243 plasma binding is high or low affinity.

Discussion

While studies in the Syrian Golden Hamster have demonstrated effectiveness of favipiravir against SARS-CoV-2, *in vitro* activity data generated in the Vero-E6 cell model have questioned the utility of the molecule when the derived target concentrations are compared to the pharmacokinetics after administration to humans. Ultimately, robustly designed and executed clinical trials will be required to determine the utility of favipiravir for SARS-CoV-2 but understanding the mechanisms which underpin the clinical pharmacology is important to understand the plausibility for evaluation, which should underpin selection of candidates for clinical evaluation. Furthermore, an *a priori* understanding of likelihood of success for future candidates can only evolve from a thorough understanding of the PKPD rules of engagement for SARS-CoV-2, which currently do not exist. Antiviral drugs have only thus far been unequivocally successful for other viruses when given in combination, and the requirement of combinations to improve potency and/or stem emergence of resistance requires careful consideration so as not to obviate the lessons that should be learned from other pathogens. Notwithstanding, favipiravir has been evaluated at several different doses and schedules in numerous clinical trials globally, with mixed outcomes [23-25]. As of 29th December 2020, a total of 44 trials were listed on clinicaltrials.gov aiming to evaluate favipiravir, predominantly as a monotherapy (with some exceptions) and in various use cases.

The current analysis aimed to apply a PK modelling approach to better understand the potential efficacy of favipiravir for SARS-CoV-2 at doses readily achievable in humans. The simulations synthesised available data for intracellular kinetics of FAVI-RTP in MDCK cells, plasma pharmacokinetics in a Chinese patient population, *in vitro*-derived antiviral activity data (EC_{90}), and cell-free inhibition data for FAVI-RTP against the SARS-CoV-2 RNA polymerase. Importantly, this modelling approach indicates that despite rapid clearance of the parent drug from plasma, the peak to trough variability in intracellular FAVI-RTP is such that activity may be maintained across the dosing interval because of the long intracellular half-life. The simulations indicate that the population average intracellular FAVI-RTP concentrations will maintain its Km for the SARS-CoV-2 polymerase for 3 days following 800 mg BID dosing and 9 days following 1200 mg BID dosing after a 1600 mg BID loading dose on day 1. Importantly, the flatter intracellular pharmacokinetic profile of the phosphorylated form of favipiravir is in keeping with observations for other antiviral nucleoside/nucleotide analogues such as tenofovir-diphosphate [26, 27], which underpins the efficacy of these drugs for other viruses.

The current approach has several important limitations that should be recognised. Favipiravir pharmacokinetic exposures have been demonstrated to be lower in American and African patients than in Chinese patients [28], and so the simulations may not be widely applicable across different ethnicities. The modelling applied a direct *in vitro* to *in vivo* extrapolation of k_{in} and this should be considered as a major assumption as it directly presumes the *in vitro* $Favi_{media}$ concentration is representative of free plasma concentration as derived from the PK model and that the umbrella k_{in} parameter, which consolidates various underlying uptake and conversion processes, is directly translatable. Importantly, the presented intracellular predictions are specific to data generated on intracellular kinetics in MDCK cells. Therefore, accuracy of the intracellular FAVI-RTP concentrations will be dependent upon the similarity of relevant human *in vivo* cells in terms of the *in vitro* uptake/elimination as well as the rate and extent of metabolic activation of favipiravir to its triphosphorylated active form. Furthermore, there are no data with which to model the inter-patient variability in the intracellular uptake or conversion to FAVI-RTP and so intracellular concentration variability shown in Figure 3 is only derived from intracellular variability in plasma exposure. Finally, the intracellular prediction is driven by the estimated free plasma concentration, whereas *in vivo* it is possible local tissue free drug concentrations at the target organ for which there are no available data may be higher or lower than in plasma.

Despite these limitations, additional confidence in the predictions come from two important sources. Firstly, following the first day of dosing, there is generally good agreement between the point at which the plasma favipiravir concentrations intersect the *in vitro* derived EC_{90} and the corresponding intracellular FAVI-RTP value being close to its Km value derived separately in a cell-free system with the SARS-CoV-2 polymerase (Figure 3). It should be noted that no data are available with which to derive a protein-adjusted EC_{90} value for favipiravir. Secondly, the clear activity of favipiravir in the Syrian Golden Hamster model when C_{trough} values are similar to those in humans gives additional confidence in the predictions [16].

In summary, these simulations indicate that favipiravir maintenance doses between 800 mg and 1200 mg BID may be sufficient to provide therapeutic concentrations of the intracellular FAVI-RTP metabolite across the dosing interval. Further evaluation of favipiravir as an antiviral for SARS-CoV-2 appears to be warranted and will provide additional clarity on its putative utility. However, the recent emergence of variants of the virus requires careful consideration of the drug resistance threat posed by using repurposed agents as monotherapies, particularly when they are likely not to be fully active in all patients. The polymerase, along with the protease and spike are likely to be extremely

311 important drug targets for new chemical entities and care should be taken not to compromise their

312 utility before the first-generation specific SARS-CoV-2 antivirals emerge.

Acknowledgements

The Authors wish to thank Professor Leon Aarons (University of Manchester) for helpful discussions during development of this work.

317

318 **Figure Captions:**

319 **Figure 1**

320 PK model fittings to time courses of $[FAVI\text{-}RTP]_{intracellular}$ generated by Smee et al. in MDCK

321 monolayers

322

323

324 **Figure 2**

325 Log-linear fitting to k_{in} as a function media favipiravir concentration

326

327

328 **Figure 3**

329 Favipiravir Plasma and Intracellular concentration predictions based on the Population-PK model of

330 Wang et al. combined with *in-vitro* intracellular PK modelling, for a dosing regimen of 1600 mg BID

331 loading dose for day 1, followed by 800 mg BID maintenance dosing for 9 further days (A), or 1600

332 mg BID loading dose for day 1, followed by 1200 mg BID maintenance dosing for 9 further days (B).

333 Dashed red line represents the previously published Km for inhibition of SARS-CoV-2 polymerase by

334 FAVI-RTP [18], dotted red line represents C_{trough} plasma concentrations of favipiravir following 1000

335 mg/kg/day dose in hamster [16] and solid red line represents the *in vitro* EC_{90} of favipiravir against

336 SARS-CoV-2 in Vero-E6 cells [14].

337

338 **Figures**

339 **Figure 1**

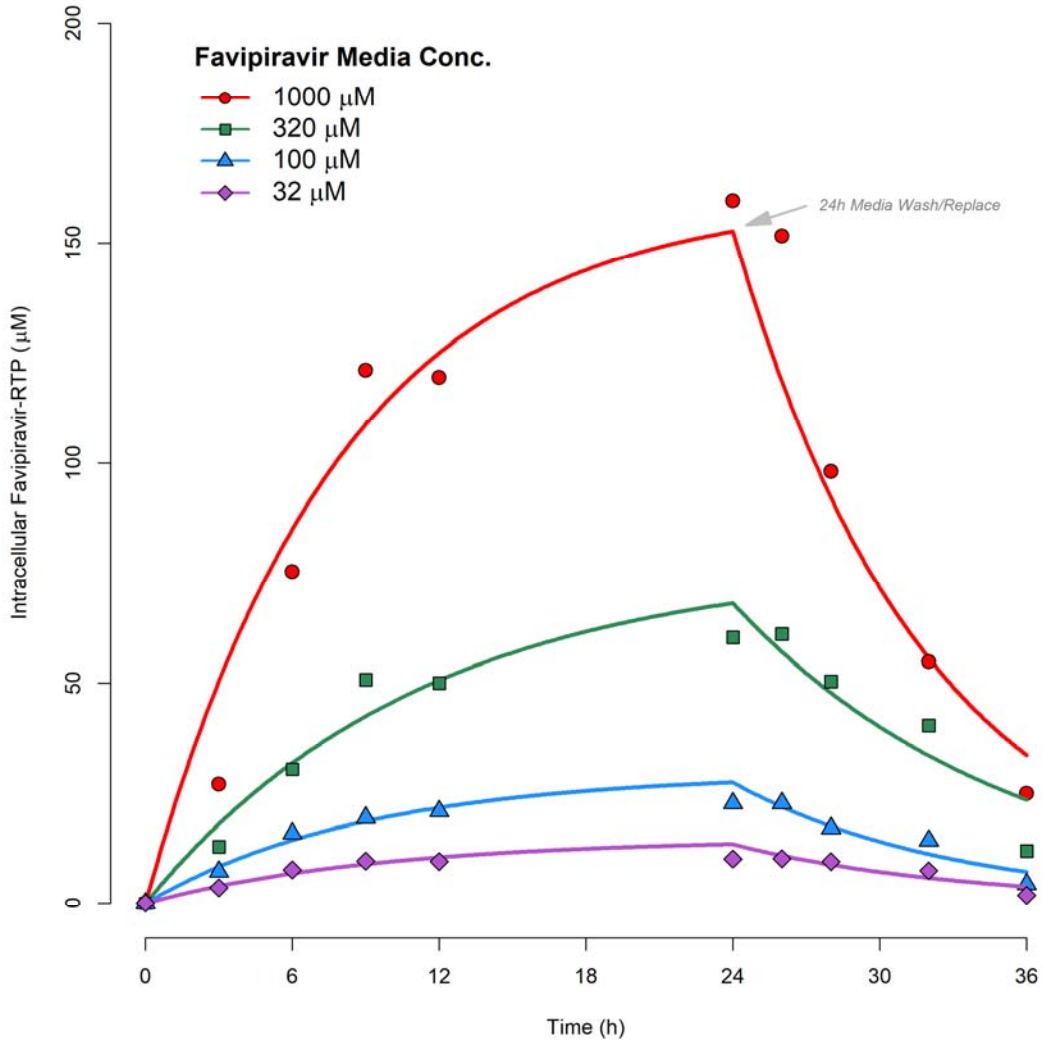

340

341

342 **Figure 2**

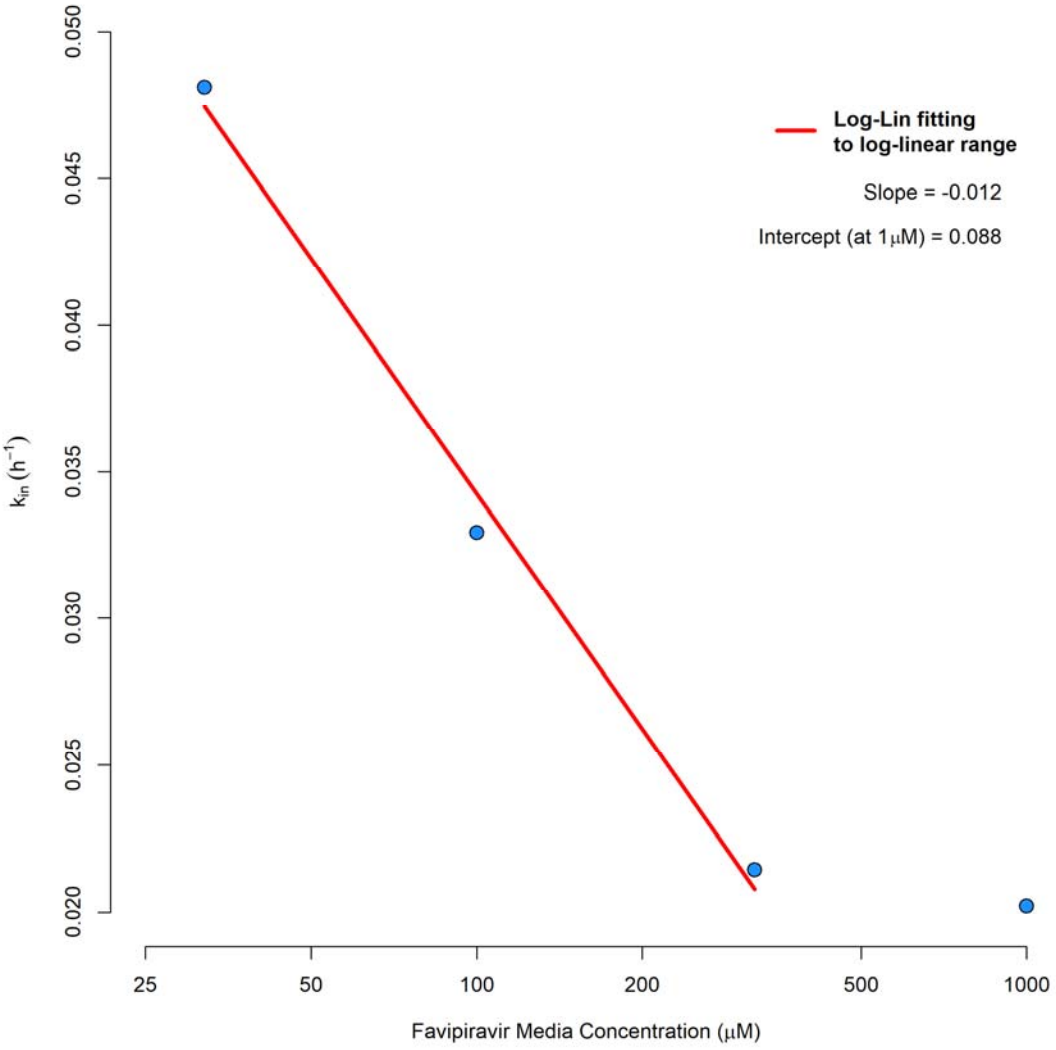

343

344

345 **Figure 3**

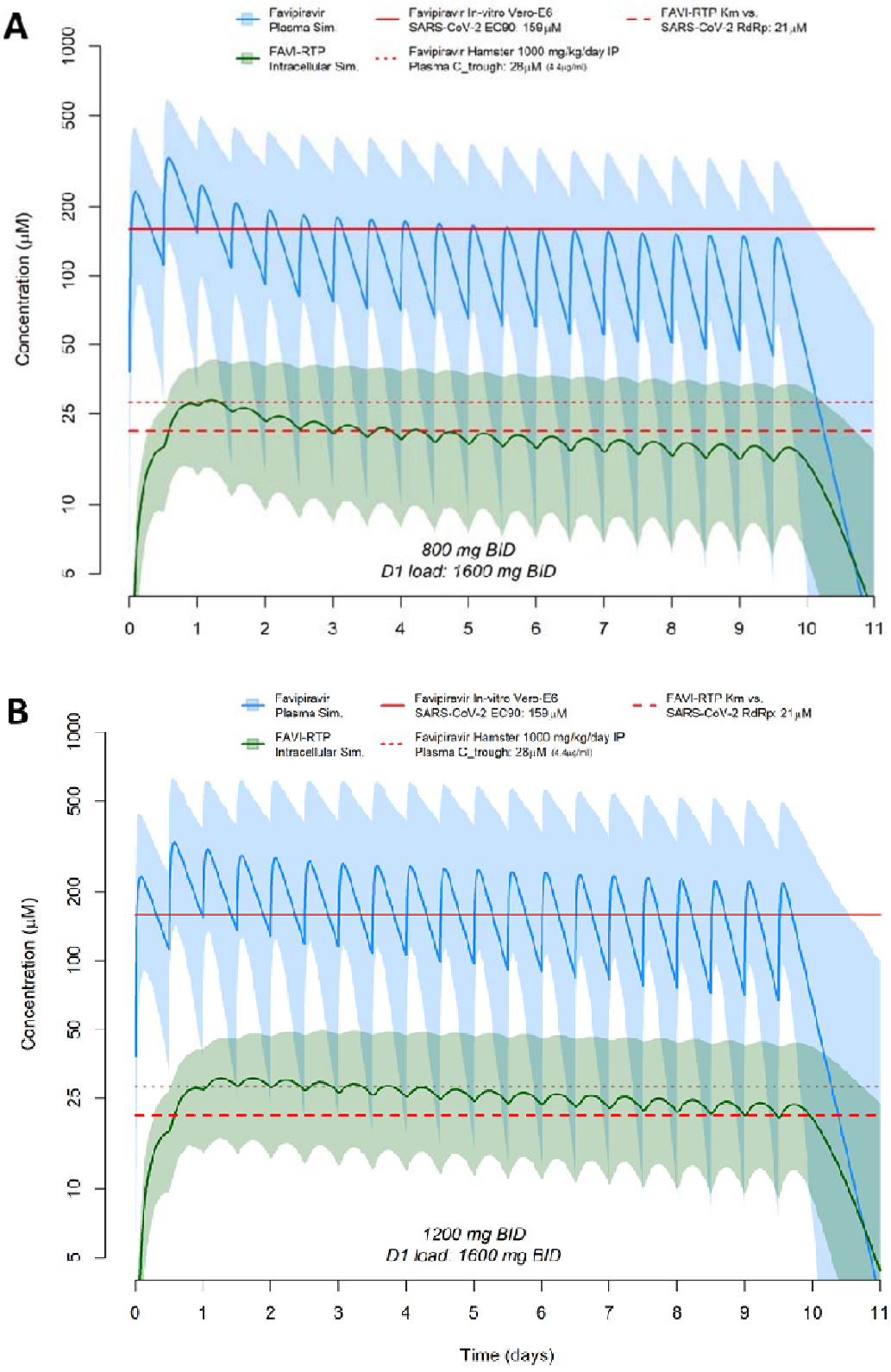

346

347 **Tables**

348 **Table 1**

349 Parameter estimates from *in vitro* PK model fittings

350

$[FAVI]_{media}$		k_{in} (h^{-1})	k_{out} (h^{-1})
1000 µM	Est.	0.020	0.126
	%RSE	13.9	11.4
320 µM	Est.	0.021	0.089
	%RSE	14.7	15.6
100 µM	Est.	0.033	0.112
	%RSE	12.0	10.7
32 µM	Est.	0.048	0.105
	%RSE	15.3	14.3

351

352

353 **Table 2**

354 Summary of favipiravir POP-PK model parameter estimates used for simulation, from Wang et. al.

355

Parameter	Est.	Inter-Individual Variance (ω^2, log parameters)
F (apparent, fractional)	1 (fixed)	0.0921
k_a (h^{-1})	1.5	1.05
CL/F (L/h)	2.96	0.274
V/F (L)	37.1	0.128
Time dep. Eff. On CL/F (% per day)	6.14	-
Interindividual Covariance for ka and V/F ($\omega^2_{ka} \sim \omega^2_{V/F}$)	-	0.23

356

357

References

1. Venisse, N., et al., *Concerns about pharmacokinetic (PK) and pharmacokinetic-pharmacodynamic (PK-PD) studies in the new therapeutic area of COVID-19 infection.* Antiviral Res, 2020. **181**: p. 104866.
2. Alexander, S.P.H., et al., *A rational roadmap for SARS-CoV-2/COVID-19 pharmacotherapeutic research and development: IUPHAR Review 29.* Br J Pharmacol, 2020. **177**(21): p. 4942-4966.
3. Arshad, U., et al., *Prioritization of Anti-SARS-Cov-2 Drug Repurposing Opportunities Based on Plasma and Target Site Concentrations Derived from their Established Human Pharmacokinetics.* Clin Pharmacol Ther, 2020. **108**(4): p. 775-790.
4. Boffito, M., et al., *Toward Consensus on Correct Interpretation of Protein Binding in Plasma and Other Biological Matrices for COVID-19 Therapeutic Development.* Clin Pharmacol Ther, 2020.
5. Owen, A. and S.H. Khoo, *Intracellular pharmacokinetics of antiretroviral agents.* J HIV Ther, 2004. **9**(4): p. 97-101.
6. Back, D.J., et al., *The pharmacology of antiretroviral nucleoside and nucleotide reverse transcriptase inhibitors: implications for once-daily dosing.* J Acquir Immune Defic Syndr, 2005. **39 Suppl 1**: p. S1-23, quiz S24-25.
7. Callebaut, C., et al., *In Vitro Virology Profile of Tenofovir Alafenamide, a Novel Oral Prodrug of Tenofovir with Improved Antiviral Activity Compared to That of Tenofovir Disoproxil Fumarate.* Antimicrob Agents Chemother, 2015. **59**(10): p. 5909-16.
8. German, P., et al., *Clinical Pharmacokinetics and Pharmacodynamics of Ledipasvir/Sofosbuvir, a Fixed-Dose Combination Tablet for the Treatment of Hepatitis C.* Clin Pharmacokinet, 2016. **55**(11): p. 1337-1351.
9. Ko, W.C., et al., *Arguments in favour of remdesivir for treating SARS-CoV-2 infections.* Int J Antimicrob Agents, 2020. **55**(4): p. 105933.
10. Hayden, F.G. and N. Shindo, *Influenza virus polymerase inhibitors in clinical development.* Curr Opin Infect Dis, 2019. **32**(2): p. 176-186.
11. Choi, S.W., et al., *Antiviral activity and safety of remdesivir against SARS-CoV-2 infection in human pluripotent stem cell-derived cardiomyocytes.* Antiviral Res, 2020. **184**: p. 104955.
12. Hattori, S.I., et al., *GRL-0920, an Indole Chloropyridinyl Ester, Completely Blocks SARS-CoV-2 Infection.* mBio, 2020. **11**(4).
13. Choy, K.T., et al., *Remdesivir, lopinavir, emetine, and homoharringtonine inhibit SARS-CoV-2 replication in vitro.* Antiviral Res, 2020. **178**: p. 104786.

14. Wang, M., et al., *Remdesivir and chloroquine effectively inhibit the recently emerged novel coronavirus (2019-nCoV) in vitro.* Cell Res, 2020. **30**(3): p. 269-271.
15. Irie, K., et al., *Pharmacokinetics of Favipiravir in Critically Ill Patients With COVID-19.* Clin Transl Sci, 2020. **13**(5): p. 880-885.
16. Kaptein, S.J.F., et al., *Favipiravir at high doses has potent antiviral activity in SARS-CoV-2-infected hamsters, whereas hydroxychloroquine lacks activity.* Proc Natl Acad Sci U S A, 2020. **117**(43): p. 26955-26965.
17. Wang, Y., et al., *Phase 2a, open-label, dose-escalating, multi-center pharmacokinetic study of favipiravir (T-705) in combination with oseltamivir in patients with severe influenza.* EBioMedicine, 2020. **62**: p. 103125.
18. Gordon, C.J., et al., *Remdesivir is a direct-acting antiviral that inhibits RNA-dependent RNA polymerase from severe acute respiratory syndrome coronavirus 2 with high potency.* J Biol Chem, 2020. **295**(20): p. 6785-6797.
19. Smee, D.F., et al., *Intracellular metabolism of favipiravir (T-705) in uninfected and influenza A (H5N1) virus-infected cells.* J Antimicrob Chemother, 2009. **64**(4): p. 741-6.
20. Bittermann, K. and K.U. Goss, *Predicting apparent passive permeability of Caco-2 and MDCK cell-monolayers: A mechanistic model.* PLoS One, 2017. **12**(12): p. e0190319.
21. Team, R.C., *R: A language and environment for statistical computing. R Foundation for Statistical Computing, Vienna, Austria.* https://www.R-project.org/. 2020.
22. Borchers, H.W., *pracma: Practical Numerical Math Functions. R package version 2.2.9.* https://CRAN.R-project.org/package=pracma. 2019.
23. Doi, Y., et al., *A Prospective, Randomized, Open-Label Trial of Early versus Late Favipiravir Therapy in Hospitalized Patients with COVID-19.* Antimicrob Agents Chemother, 2020. **64**(12).
24. Ivashchenko, A.A., et al., *AVIFAVIR for Treatment of Patients with Moderate COVID-19: Interim Results of a Phase II/III Multicenter Randomized Clinical Trial.* Clin Infect Dis, 2020.
25. Prakash, A., et al., *Systematic review and meta-analysis of effectiveness and safety of favipiravir in the management of novel coronavirus (COVID-19) patients.* Indian J Pharmacol, 2020. **52**(5): p. 414-421.
26. Hawkins, T., et al., *Intracellular pharmacokinetics of tenofovir diphosphate, carbovir triphosphate, and lamivudine triphosphate in patients receiving triple-nucleoside regimens.* J Acquir Immune Defic Syndr, 2005. **39**(4): p. 406-11.
27. Baheti, G., et al., *Plasma and intracellular population pharmacokinetic analysis of tenofovir in HIV-1-infected patients.* Antimicrob Agents Chemother, 2011. **55**(11): p. 5294-9.

425 28. Nguyen, T.H., et al., *Favipiravir pharmacokinetics in Ebola-Infected patients of the JIKI trial*
426 *reveals concentrations lower than targeted.* PLoS Negl Trop Dis, 2017. **11**(2): p. e0005389.
427